Ab initio Lattice Thermal Conductivity of $MgSiO_3$ Perovskite as Found in Earth's Lower Mantle

Haruhiko Dekura (出倉春彦),[1] Taku Tsuchiya (土屋卓久),[2] and Jun Tsuchiya (土屋旬)[1]
[1]*Senior Research Fellow Center, Ehime University, 2-5 Bunkyo-cho, Matsuyama 790-8577, Japan*
[2]*Geodynamics Research Center, Ehime University, 2-5 Bunkyo-cho, Matsuyama 790-8577, Japan*
(Received 23 July 2012; published 11 January 2013)

The lattice thermal conductivity ($\kappa_{\rm lat}$) of $MgSiO_3$ perovskite (Mg-Pv) under high-pressure and high-temperature conditions was computed based on the *ab initio* anharmonic lattice dynamics method with the density functional perturbation theory. $\kappa_{\rm lat}$ of Mg-Pv is found to increase with increasing pressure from 9.8 (at 23.5 GPa) to 43.6 $\mathrm{W\,m^{-1}\,K^{-1}}$ (at 136 GPa) at 300 K, while decreasing with increasing temperature from 28.1 (at 300 K) to 2.3 $\mathrm{W\,m^{-1}\,K^{-1}}$ (at 4000 K) at 100 GPa. A multiphase composite average yielded a mantle Rayleigh number adequate to promote the vigorous thermal convection of the mantle that is expected geophysically.

DOI: 10.1103/PhysRevLett.110.025904 PACS numbers: 66.70.Lm, 62.50.−p, 63.20.kg, 91.35.Gf

Thermal conductivity (κ) is a fundamental physical parameter in controlling the heat transfer in Earth's interior. Despite its importance, the thermal conductivity of mantle minerals has long been one of the properties most unconstrained at high pressure (P) and high temperature (T), particularly owing to experimental difficulty. κ of Earth's lower mantle (LM) minerals has therefore often been inferred by extrapolating limited number of data measured at low-P, T conditions [1–4]. Large extrapolations to high-P, T conditions, however, cause significant uncertainties at deep mantle conditions. For κ of $MgSiO_3$ perovskite (Mg-Pv), thought to be a dominant mineral phase in the LM ($P \sim 24$–135 GPa, $T \sim 2000$–4000 K), Osako reported 5.1 $\mathrm{W\,m^{-1}\,K^{-1}}$ at ambient pressure and room temperature [1]. Recently, a high-pressure study using a multianvil press [3] measured 15.6 $\mathrm{W\,m^{-1}\,K^{-1}}$ at 26 GPa at 473 K, which decreased to 10.4 $\mathrm{W\,m^{-1}\,K^{-1}}$ with increasing temperature to 1073 K. Although a diamond-anvil cell study [4] extended the pressure condition up to 144 GPa, the reported κ is inconsistent with the values above and is much smaller-it is 10.6 $\mathrm{W\,m^{-1}\,K^{-1}}$ even at 31 GPa and room temperature.

Ab initio theory has also been extended recently to evaluate the lattice thermal conductivity ($\kappa_{\rm lat}$) of minerals. That of MgO was calculated based on the anharmonic lattice dynamics [5], the equilibrium molecular dynamics [6,7]], and the nonequilibrium molecular dynamics [8] methods. These studies reproduced low-P experimental values [2] fairly well and predicted comparable values of 30–50 $\mathrm{W\,m^{-1}\,K^{-1}}$ at deep LM conditions of 136 GPa and 2500 K. However, all these techniques generally have difficulties for sufficient sampling of phonons with long wavelengths comparable to their mean-free paths, unless adopting an impractically large supercell. In contrast, phonon lifetimes (τ) of Si and Ge were computed by a more sophisticated approach, where the third-order dynamical tensor was computed at an arbitrary wave vector ($\mathbf{q}$) with a primitive cell based on the perturbation approach [9–11]. Predicted $\kappa_{\rm lat}$ agree excellently with experiments, suggesting substantial prospects for other compounds. In this study, we calculate τ of Mg-Pv based on this technique and determine $\kappa_{\rm lat}$ nonempirically in a wide P, T range covering the entire LM conditions for the first time.

The intrinsic bulk thermal conduction of insulators is caused by anharmonic phonon-phonon interactions, and thus evaluation of the anharmonic coupling strength is a key to calculating $\kappa_{\rm lat}$. Within the single-mode relaxation time approximation for the phonon Boltzmann's transport equation [12], $\kappa_{\rm lat}$ is given by

$$\kappa_{\rm lat} = \frac{1}{3}\sum_s \int |\mathbf{v}_{\mathbf{q},s}|^2 c_{\mathbf{q},s}\tau_{\mathbf{q},s} d\mathbf{q}, \quad (1)$$

where $\mathbf{v}_{\mathbf{q},s}$, $c_{\mathbf{q},s}$, and $\tau_{\mathbf{q},s}$ are the phonon group velocity, the mode heat capacity, and the phonon lifetime at $\mathbf{q}$ for the branch s, respectively. $\tau_{\mathbf{q},s}$ is related to the phonon damping function $\Gamma_{\mathbf{q},s} = 1/2\tau_{\mathbf{q},s}$ that measures the lattice anharmonicity attributable to phonon-phonon interactions. When considering up to the three phonon process, which is sufficient for ionic and covalent crystals with no soft phonon modes like silicon, diamond, MgO [5,11,13,14], the frequency dependent dumping function for a phonon at $\mathbf{q}$ is represented by

$$\begin{aligned}\Gamma_{\mathbf{q},s}(\omega) = \frac{\pi}{2N_{\mathbf{q}'}}\sum_{\mathbf{q}',s',s''} &|V_3(\mathbf{q}s, \mathbf{q}'s', \mathbf{q}''s'')|^2 \\ &\times [\{1 + n_{\mathbf{q}',s'} + n_{\mathbf{q}'',s''}\}\delta(\omega_{\mathbf{q}',s'} + \omega_{\mathbf{q}'',s''} - \omega) \\ &+ 2\{n_{\mathbf{q}'',s''} - n_{\mathbf{q}',s'}\}\delta(\omega_{\mathbf{q}',s'} - \omega_{\mathbf{q}'',s''} - \omega)], \quad (2)\end{aligned}$$

where $n_{\mathbf{q},s} = 1/(e^{\hbar\omega_{\mathbf{q},s}/k_BT} - 1)$ is the Bose-Einstein occupation number for a phonon with energy $\hbar\omega_{\mathbf{q},s}$, $V_3(\mathbf{q}s, \mathbf{q}'s', \mathbf{q}''s'')$ is the anharmonic three-phonon coupling coefficient for the creation and annihilation process described in square brackets, and $N_{\mathbf{q}'}$ is the number of $\mathbf{q}$-points sampled in the integration [10]. Due to the umklapp quasimomentum conservation,

$\mathbf{q}'' = -\mathbf{q} - \mathbf{q}' + \mathbf{G}$. The first and second terms in the square brackets represent the so-called summation process ($D^{\uparrow}$)—decay of a single phonon into two phonons with lower frequencies-and the so-called difference process ($D^{\downarrow}$)—up conversion of two phonons into a single phonon with higher energy, respectively. $V_3(\mathbf{q}s, \mathbf{q}'s', \mathbf{q}''s'')$ is further represented as

$$V_3(\mathbf{q}s, \mathbf{q}'s', \mathbf{q}''s'') = \sqrt{\hbar/8\omega_{\mathbf{q},s}\omega_{\mathbf{q}',s'}\omega_{\mathbf{q}'',s''}} \times \sum_{\kappa\alpha,\kappa'\alpha',\kappa''\alpha''} \Psi^{\kappa\kappa'\kappa''}_{\alpha\alpha'\alpha''}(\mathbf{q}, \mathbf{q}', \mathbf{q}'') \times \frac{e^{\kappa}_{\alpha}(\mathbf{q}, s)e^{\kappa'}_{\alpha'}(\mathbf{q}', s')e^{\kappa''}_{\alpha''}(\mathbf{q}'', s'')}{\sqrt{M_{\kappa}M_{\kappa'}M_{\kappa''}}} \times e^{i(\mathbf{q}\cdot\mathbf{R}+\mathbf{q}'\cdot\mathbf{R}'+\mathbf{q}''\cdot\mathbf{R}'')}, \quad (3)$$

where the summation is taken over indices of atom κ and component α. $\Psi^{\kappa\kappa'\kappa''}_{\alpha\alpha'\alpha''}(\mathbf{q}, \mathbf{q}', \mathbf{q}'')$ is the third-order anharmonic dynamical tensor, which can be calculated based on the density functional perturbation theory combined with the $2n + 1$ theorem [9,10,15,16].

The damping function in Eq. (2) is related to the temperature dependent two-phonon density of states (TDoS) that measures the number of damping channels for the $D^{\uparrow}$ and $D^{\downarrow}$ processes, which are represented for $\mathbf{q} = \vec{\mathbf{0}}$ as

$$D^{\uparrow}_{\mathbf{q}=\vec{\mathbf{0}}}(\omega) = \frac{1}{N_{\mathbf{q}'}} \sum_{\mathbf{q}',j,j'} \{1 + n_{\mathbf{q}',j} + n_{-\mathbf{q}',j'}\} \times \delta(\omega_{\mathbf{q}',j} + \omega_{-\mathbf{q}',j'} - \omega) \quad (4)$$

and

$$D^{\downarrow}_{\mathbf{q}=\vec{\mathbf{0}}}(\omega) = \frac{1}{N_{\mathbf{q}'}} \sum_{\mathbf{q}',j,j'} 2\{n_{-\mathbf{q}',j'} - n_{\mathbf{q}',j}\} \times \delta(\omega_{\mathbf{q}',j} - \omega_{-\mathbf{q}',j'} - \omega) \quad (5)$$

respectively. The TDoS of Mg-Pv calculated as a function of frequency at $T = 300$ K at $V = 24.04$ cm^3 mol^{-1} and 18.88 cm^3 mol^{-1}, corresponding to static pressures of 0 GPa and 100 GPa respectively, are shown in Fig. 1(a). Detailed conditions for the calculations are given in supplementary materials [16]. The results show that the contributions of $D^{\uparrow}$ (dotted lines) and $D^{\downarrow}$ (dashed lines) dominate the decay of phonons with relatively high and low frequencies, respectively. This is based clearly on the energy conservation through the phonon-phonon scattering. It is also seen that $D^{\uparrow}_{\mathbf{q}=\vec{\mathbf{0}}}(\omega)$ and $D^{\downarrow}_{\mathbf{q}=\vec{\mathbf{0}}}(\omega)$ in the one-phonon regime (the harmonic frequency range up to the highest modes) both decrease with increasing pressure, meaning that the number of decay channels decreases under compression, and thus the phonon lifetimes in contrast increase. Figure 1(a) also shows that the $D^{\uparrow}$ process starts to increase from ~250 cm^{-1} and ~350 cm^{-1} at 0 and 100 GPa, respectively. These frequencies correspond to the lowest optic phonon frequencies at each pressure,

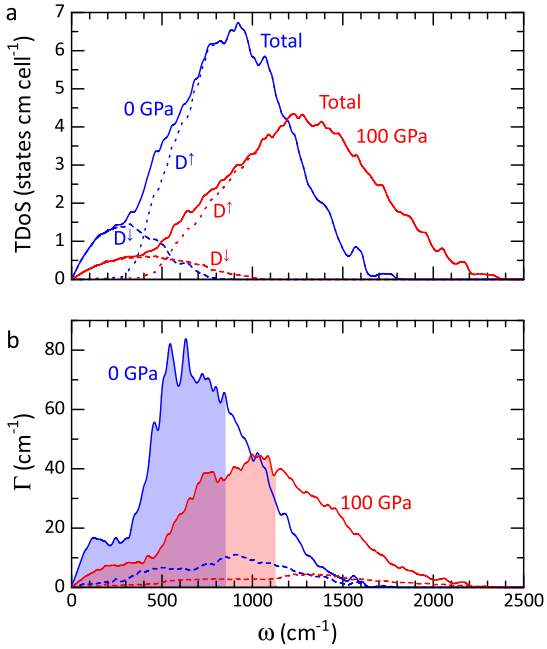

FIG. 1 (color online). Calculated anharmonic properties of Mg-Pv. (a) TDoS for the total (solid lines), the summation $D^{\uparrow}_{\mathbf{q}=\vec{\mathbf{0}}}$ Eq. (4) (dotted lines), and the difference process $D^{\downarrow}_{\mathbf{q}=\vec{\mathbf{0}}}(\omega)$ Eq. (5) (dashed lines). (b) Damping function $\Gamma_{\mathbf{q}=\vec{\mathbf{0}}}$ Eq. (2) of the lowest (solid lines) and the highest optic phonon branches (dashed lines) at 300 K, which have harmonic frequencies of 186.9 and 852.4 cm^{-1} at 0 GPa and 235.1 and 1127.3 cm^{-1} at 100 GPa, respectively. Shaded areas represent $\Gamma_{\mathbf{q}=\vec{\mathbf{0}}}$ below the highest phonon frequencies.

indicating that the optic phonon scattering dominates $D^{\uparrow}$ while the acoustic modes mostly contribute to $D^{\downarrow}$. In Mg-Pv, the number of the optic phonon branches (57) is much larger than that of the acoustic branches (3). Therefore, the $D^{\uparrow}$ process is found to have much larger TDoS than $D^{\downarrow}$. This behavior is clearly different from simple crystals llike MgO [5]. The damping functions $\Gamma_{\mathbf{q}=\vec{\mathbf{0}}}(\omega)$ for all the phonon branches were then calculated, and those of the lowest and highest optic phonon modes are shown in Fig. 1(b). They are found to decrease with increasing pressure, reflecting the behavior of TDoS and clearly indicating an increase in $\tau_{\mathbf{q}=\vec{\mathbf{0}}}$ with pressure. This figure also shows that the lowest optic branch (solid lines) is more easily damped than the highest branch (dashed lines). As shown in Eq. (2), Γ is related to the TDoS and weighted by the anharmonic coupling coefficient V_3. The larger Γ of the lowest optic branch is therefore due to a larger V_3.

Using the calculated $\tau_{\mathbf{q},s}$ and harmonic properties [16], $\kappa_{\mathrm{lat}}(V, T)$ was determined as a function of volume and temperature as demonstrated in Fig. 2(a). The volume range here corresponds to the static pressure from −10 to 210 GPa. Obtained results were well fitted to the following analytical function,

$$\kappa_{\rm lat}(V,T) = \kappa_0 x^q \frac{1-e^{-a_3 T_0/T}}{1-e^{-a_3}}, \quad (6)$$

where $x \equiv V/V_0$, and $q \equiv a_1 + a_2 x$. κ_0 and $a_1 \sim a_3$ are the fitting parameters determined as $\kappa_0 = 6.7 \pm 1.0$ W m^{-1} K^{-1}, $a_1 = -13.4 \pm 1.7$, $a_2 = 10.1 \pm 2.8$, and $a_3 = 1.1 \pm 0.3$. $V_0 = 24.71$ cm^3 mol^{-1} is the volume at 0 GPa and 300 K [17], and $T_0 = 300$ K. This fitting produced a root-mean-square (rms) error of ± 1.3 W m^{-1} K^{-1} corresponding to a relative error of 15%. The exponential term representing the temperature effect is related to the inverse of the Bose-Einstein function, which can describe both the low-T quantal behavior and the high-T behavior asymptotic to T^{-1} appropriately. A simpler form used in some geophysical studies [18],

$$\kappa_{\rm lat}(V,T) = \kappa_0 \left(\frac{V}{V_0}\right)^{-a} \left(\frac{T_0}{T}\right) \quad (7)$$

was also examined, where κ_0 and a are the fitting parameters. This provided $\kappa_0 = 4.7 \pm 1.3$ W m^{-1} K^{-1} and $a = 8.0 \pm 0.5$ but a notably larger rms error of ± 2.5 W m^{-1} K^{-1} corresponding to a relative error as much as 30%, indicating that our formula Eq. (6) is more suitable to represent $\kappa_{\rm lat}$ in a wide P,T range from ambient condition up to ~200 GPa and ~4000 K. The obtained analytical representation of $\kappa_{\rm lat}(V,T)$ was then converted to the $\kappa_{\rm lat}(P,T)$ data set by using the thermal equation of state of Mg-Pv [17,19]. Figure 2(b) shows the pressure dependence of $\kappa_{\rm lat}$ at several temperatures, clearly indicating that $\kappa_{\rm lat}$ substantially increases with increasing pressure. The calculated $\kappa_{\rm lat}$ at 0 GPa and 300 K (6.7 W m^{-1} K^{-1}) is found to be in excellent agreement with the experimental value (5.1 W m^{-1} K^{-1}) [1]. The high-pressure values also agree acceptably with the room-temperature experimental results [4], while the present calculations suggest that some overestimations are expected in the high-temperature measurements at 26 GPa [3]. The discrepancies between calculations and experiments in the former case are mostly within experimental error (Fig. 2(b)).

Next, we model the total thermal conductivity of the actual LM ($\kappa_{\rm LM}$) as follows. (1) The LM can be approximated as an Mg-Pv + MgO two-phase mixture with a pyrolitic ratio (8:2 in volume) [20]. A composite average was taken based on the Hashin-Shtrikman equation [21] using the $\kappa_{\rm lat}$ of MgO recently reported [8]. (2) At mantle conditions, iron is known to dissolve into both Pv and MgO to form solid solutions (Mg, Fe)SiO$_3$ and (Mg,Fe)O. Substantial reductions on $\kappa_{\rm lat}$ approximately by half in Pv and by one third in MgO were recently measured for the phases with 3 and 20 mol% iron, respectively [3], based on which we modeled the effects of iron on $\kappa_{\rm lat}$ [16]. (3) Other scatterers such as grain boundary and point defects including isotopes are not taken into account in this study, since their effects are likely expected to be marginal at LM temperatures [22]. (4) In contrast, the

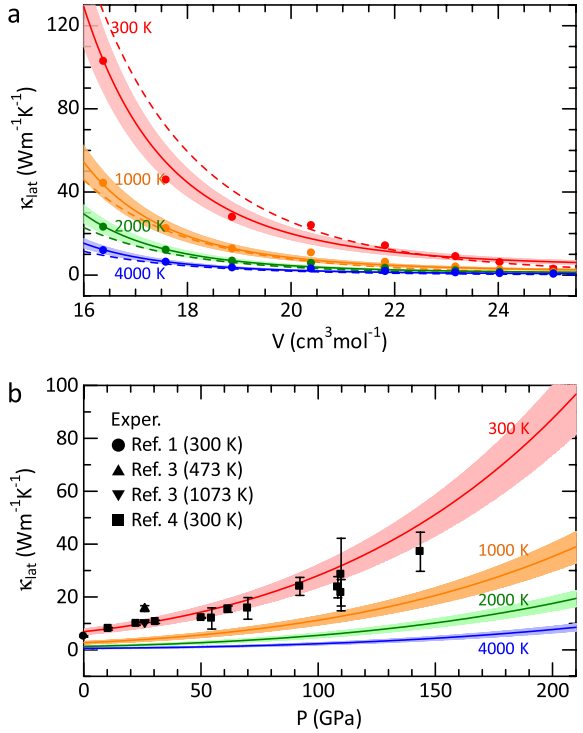

FIG. 2 (color online). Calculated $\kappa_{\rm lat}$ of Mg-Pv. (a) Volume dependence of $\kappa_{\rm lat}$ at several temperatures from 300 K to 4000 K with regression curves to Eq. (6). (b) $\kappa_{\rm lat}$ converted to a function of pressure with experimental data (filled symbols) [1,3,4].

radiative energy transportation $\kappa_{\rm rad}$, also not calculated in this study, is generally thought to increase at high temperature. Although $\kappa_{\rm rad}$ of Mg-Pv and MgO are currently only roughly constrained at deep mantle conditions [23–26], we employ $\kappa_{\rm rad}(T) = \chi T^3$ with $\chi = 8.5 \times 10^{-11}$ W m^{-1} K^{-4} proposed for dense silicates and oxides [25].

$\kappa_{\rm LM}$ obtained based on this analysis is plotted as a function of pressure and temperature in Fig. 3. The strong positive pressure dependence of $\kappa_{\rm LM}$ is found at low temperatures as the $\kappa_{\rm lat}$ of Mg-Pv. However, $\kappa_{\rm LM}$ also increases with temperature due to the increase in radiative conductivity at high temperature. Figure 3 suggests that this contribution is not negligible at the deepest mantle conditions. The change in $\kappa_{\rm LM}$ is consequently found from 1.39 to 4.46 W m^{-1} K^{-1} along the LM adiabat [27] from the top of the LM at $z = 660$ km depth ($P \sim 23.5$ GPa, $T \sim 1880$ K) to the base at $z = 2890$ km depth ($P \sim 136$ GPa, $T \sim 2450$ K), where $X_{\rm Fe} = 5$ and 20 mol% for Pv and MgO, respectively. The Rayleigh number, Ra, is a fundamental quantity specifying the style of convecting fluids, also applied to describe the Earth's mantle convection [28]. It is expressed as

$$\mathrm{Ra} = \frac{\alpha g \Delta T \rho^2 C_P z^3}{\nu \kappa}, \quad (8)$$

where α is thermal expansivity, g is acceleration of gravity, ΔT is the temperature difference between hot (upwelling)

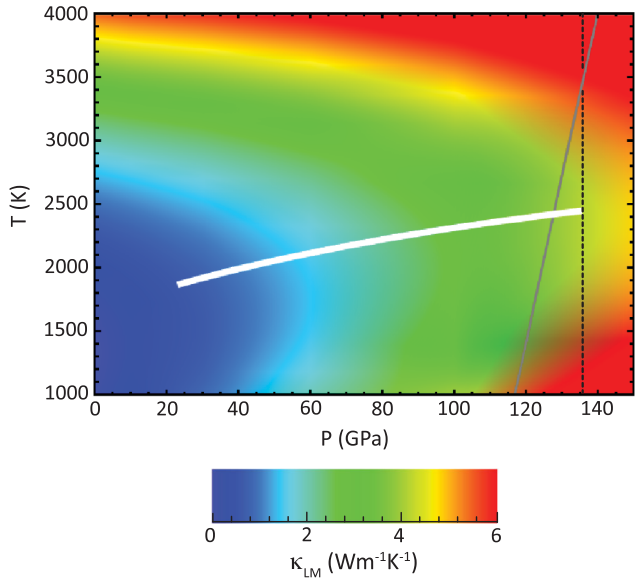

FIG. 3 (color). Pressure and temperature color contour plot of κ_{LM}. White thick and gray thin solid lines represent a typical mantle geotherm [27] and the Pv-PPv phase boundary [19], respectively. Vertical dotted line represents the CMB pressure.

and cold (downwelling) regions, ρ is density, C_P is isobaric heat capacity, z is the depth from the surface, ν is viscosity, and κ is thermal conductivity. A combination of $\kappa = 4.5\ \mathrm{W\,m^{-1}\,K^{-1}}$ obtained in this study, a typically proposed temperature difference $\Delta T = 500$ K [29], and reported values at $z = 2890$ km depth ($\alpha = 1.22 \times 10^{-5}\ \mathrm{K^{-1}}$, $C_P = 1.29\ \mathrm{Jg^{-1}\,K^{-1}}$, $\rho = 5.35\ \mathrm{gcm^{-3}}$ for the Mg-Pv + MgO mixture [17,30], $g = 10.7\ \mathrm{ms^{-2}}$ [31], and $\nu = 10^{21}$–10^{23} Pas for the Earth's LM [32]) yields Ra $\sim 10^5$–10^7. If Ra is larger than a critical value Ra_c ($\sim 10^3$–10^4 for the Earth's mantle [28]), convective energy transfer is allowed. If smaller, in contrast, the thermal energy is transported solely by conduction. The sufficiently high Ra of the LM evaluated here indicates that the Earth's mantle lies in the vigorously convective regime, which is expected geophysically [28].

The current prediction for κ_{LM} also allows us to infer the heat flow Q across the Earth's core-mantle boundary (CMB). The conductive energy flux expected across the CMB q_{CMB} can be represented based on the Fourier's heat law as $q = \kappa_{\mathrm{LM}} \Delta T/\Delta Z$. Here, we apply $\kappa_{\mathrm{LM}}(136\ \mathrm{GPa}, 3200\ \mathrm{K}) = 5.3\ \mathrm{W\,m^{-1}\,K^{-1}}$ and $\Delta T/\Delta Z = 4$–$7\ \mathrm{K\,km^{-1}}$ for the temperature gradient in the deepest mantle thermal boundary layer [29]. This leads to $q_{\mathrm{CMB}} = 0.02$–$0.04\ \mathrm{W\,m^{-2}}$, then $Q_{\mathrm{CMB}} = 4\pi r_{\mathrm{CMB}}^2 q_{\mathrm{CMB}} = 3$–$6$ TW with the Earth's core radius $r_{\mathrm{CMB}} \sim 3480$ km. This heat flow, corresponding to $\sim$10% of the surface heat flow (46 ± 3 TW) [33], is larger than that required to sustain the geodynamo at the current magnitude ($\sim$ 2–3.5 TW) [34]. However, since a high-pressure phase transition from Mg-Pv to the post-perovskite (PPv) phase is expected near the CMB [19], κ_{lat} of PPv, which is suggested to be larger than that of Pv at room temperature [4], must clearly be applied for a more accurate estimation of Q_{CMB}. The present method is widely applicable to the *ab initio* determination of the lattice thermal conductivity of other minerals including Mg-PPv.

We thank N. Yahata for preliminary computations, K. Ohta for discussion, and S. Whitaker for comments. This work was supported by special coordination funds for promoting science and technology (Supporting Young Researchers with Fixed-term Appointments) and in part by KAKENHI Nos. 20001005 and 21740379.

[1] M. Osako and E. Ito, Geophys. Res. Lett. **18**, 239 (1991).
[2] T. Katsura, Phys. Earth Planet. Inter. **101**, 73 (1997).
[3] G. M. Manthilake, N. de Koker, D. J. Frost, and C. A. McCammon, Proc. Natl. Acad. Sci. U.S.A. **108**, 17901 (2011).
[4] K. Ohta, T. Yagi, N. Taketoshi, K. Hirose, T. Komabayashi, T. Baba, Y. Ohishi, and J. Hernlund, Earth Planet. Sci. Lett. **349–350**, 109 (2012).
[5] X. Tang and J. Dong, Proc. Natl. Acad. Sci. U.S.A. **107**, 4539 (2010).
[6] N. de Koker, Phys. Rev. Lett. **103**, 125902 (2009).
[7] N. de Koker, Earth Planet. Sci. Lett. **292**, 392 (2010).
[8] S. Stackhouse, L. Stixrude, and B. B. Karki, Phys. Rev. Lett. **104**, 208501 (2010).
[9] A. Debernardi, Phys. Rev. B **57**, 12847 (1998).
[10] G. Deinzer, G. Birner, and D. Strauch, Phys. Rev. B **67**, 144304 (2003).
[11] A. Ward and D. A. Broido, Phys. Rev. B **81**, 085205 (2010).
[12] J. M. Ziman, *Electrons and Phonons* (Oxford, University Press, London, 1960).
[13] D. J. Ecsedy and P. G. Klemens, Phys. Rev. B **15**, 5957 (1977).
[14] A. Ward, D. A. Broido, D. A. Stewart, and G. Deinzer, Phys. Rev. B **80**, 125203 (2009).
[15] X. Gonze and J. P. Vigneron, Phys. Rev. B **39**, 13120 (1989).
[16] See Supplemental Material for details about the computations. For more information on Supplemental Material, see http://link.aps.org/supplemental/10.1103/PhysRevLett.110.025904.
[17] J. Tsuchiya, T. Tsuchiya, and R. M. Wentzcovitch, J. Geophys. Res. **110**, B02204 (2005).
[18] J. M. Brown, Geophys. Res. Lett. **13**, 1509 (1986).
[19] T. Tsuchiya, J. Tsuchiya, K. Umemoto, and R. M. Wentzcovitch, Earth Planet. Sci. Lett. **224**, 241 (2004).
[20] A. E. Ringwood, J. Geophys. Res. **67**, 857 (1962).
[21] Z. Hashin and S. Shtrikman, J. Appl. Phys. **33**, 3125 (1962).
[22] B. Gibert, F. R. Schilling, A. Tommasi, and D. Mainprice, Geophys. Res. Lett. **30**, 1046 (2003).
[23] H. Keppler, L. Dubrovinsky, O. Narygina, and I. Kantor, Science **322**, 1529 (2008).
[24] A. F. Goncharov, B. D. Haugen, V. V. Struzhkin, P. Beck, and S. D. Jacobsen, Nature (London) **456**, 231 (2008).

[25] A. M. Hofmeister, Science **283**, 1699 (1999).
[26] A. M. Hofmeister, Earth Planet. Sci. Lett. **170**, 201 (2008).
[27] J. M. Brown and T. J. Shankland, Geophys. J. R. Astron. Soc. **66**, 579 (1981).
[28] V. S. Solomatov and L. Moresi, Geophys. Res. Lett. **24**, 1907 (1997).
[29] K. Kawai and T. Tsuchiya, Proc. Natl. Acad. Sci. U.S.A. **106**, 22119 (2009).
[30] B. B. Karki, R. M. Wentzcovitch, S. de Gironcoli, and S. Baroni, Phys. Rev. B **61**, 8793 (2000).
[31] A. M. Dziewonski and D. L. Anderson, Phys. Earth Planet. Inter. **25**, 297 (1981).
[32] J. X. Mitrovica and A. M. Forte, Earth Planet. Sci. Lett. **225**, 177 (2004).
[33] T. Lay, J. Hernlund, and B. A. Buffett, Nat. Geosci. **1**, 25 (2008).
[34] B. A. Buffett, Geophys. Res. Lett. **29**, 1566 (2002).